Scientific Research Publishing

Journal of Water Resource and Protection, 2023, 15, 692-705
https://www.scirp.org/journal/jwarp
ISSN Online: 1945-3108
ISSN Print: 1945-3094

Flow-Induced Clogging in Microfiltration Membranes: Numerical Modeling and Parametric Study

Abdullah Rajah Al Qahtani

Department of Mechanical Skills in Jubail Technical Institute, Royal Commission of Jubail and Yanbu, Jubail, Saudi Arabia
Email: Qahtani_ab@RCJY.EDU.SA

How to cite this paper: Al Qahtani, A.R. (2023) Flow-Induced Clogging in Microfiltration Membranes: Numerical Modeling and Parametric Study. *Journal of Water Resource and Protection*, **15**, 692-705.
https://doi.org/10.4236/jwarp.2023.1512037

Received: November 12, 2023
Accepted: December 22, 2023
Published: December 25, 2023

Abstract

Microfiltration membrane technology has been widely used in various industries for solid-liquid separation. However, pore clogging remains a persistent challenge. This study employs (CFD) and discrete element method (DEM) models to enhance our understanding of microfiltration membrane clogging. The models were validated by comparing them to experimental data, demonstrating reasonable consistency. Subsequently, a parametric study was conducted on a cross-flow model, exploring the influence of key parameters on clogging. Findings show that clogging is a complex phenomenon affected by various factors. The mean inlet velocity and trans-membrane flux were found to directly impact clogging, while the confinement ratio and cosine of the membrane pore entrance angle had an inverse relationship with it. Two clog types were identified: internal (inside the pore) and external (arching at the pore entrance), with the confinement ratio determining the type. This study introduced a dimensionless number as a quantitative clogging indicator based on trans-membrane flux, Reynolds number, filtration time, entrance angle cosine, and confinement ratio. While this hypothesis held true in simulations, future studies should explore variations in clogging indicators, and improved modeling of clogging characteristics. Calibration between numerical and physical times and consideration of particle volume fraction will enhance understanding.

Keywords

Microfiltration Membrane, Parametric Study, Computational Fluid Dynamic (CFD), Discrete Element Method (DEM), CFD-DEM Modeling, Membrane Clogging, Pore Geometry, Numerical Modeling, Cake Layer, Clogging Indicator

1. Introduction

Membrane desalination has been the leading desalination technology since the beginning of the 21st century. One critical aspect of this technology is pretreatment, particularly the prefiltration of membrane feedwater. A significant challenge in this process is the clogging and formation of a cake layer on the microfiltration membrane used at this stage. In the literature, a few control methods for preventing fouling are discussed, including flux rate reduction and increased shear stress on the membrane [1]. Investigative studies emphasize the importance of understanding key factors in flow-induced clogging. A study constructed a cross-flow device with a confinement ratio of 8, revealing that trans-membrane flux is a primary clogging factor [2]. Higher flux increases in-pore clogging due to enhanced debris flow. Cross-flow influences the cake layer build-up rate, with higher cross-flow resulting in less fouling. Shear stress, not cross-flow, governs the cake layer growth rate [2]. A numerical study used "Ansys FLUENT" to predict shear stress effects. Lower shear stress leads to higher fouling rates, while higher shear stress reduces cake layer build-up [3]. Shear stress can induce clogging in neighboring pores, accelerating clogging migration Pore geometry influences clogging, with steep entrance angles promoting clogging due to the "Energy Barrier". Van der Waals and surfactant forces play a role, making clogs more likely in steep-angle pores. Shallow angles are less prone to permanent clogs [4]. Aggregated clogging results from particle-to-particle interactions at high concentrations and particle-to-wall interactions at moderate levels [5]. Particle concentration, termed the confinement ratio, affects clogging mode. Large pores relative to particle size led to inner fouling, while small pores relative to particle size cause surface fouling [6]. Various forces in fluid-particle interactions influence clogging, including drag, lift, lubrication, and other viscous forces, as well as gravitational, buoyancy, pressure gradient, and virtual mass forces [7]. These parameters are interconnected, and a flow map similar what is found in the literature could serve as a clogging identifier, based on flow velocity and particle volume fraction [8]. In **Table 1**, the flow-induced clogging factors, their impact, and the sources from which these factors are found are listed.

2. Theory

Microfluidics studies fluid flow at the microscale, typically assuming laminar

Table 1. Summary of parameters and their impacts on membrane clogging.

Factor	Impact	Source
Trans-Membrane Flux	Enhance primary clogging	[2] [3]
Mean Inlet Velocity	Reduce cake layer buildup rate, Induce pore to pore clogging	[2] [3] [4]
Pore Geometry	Influences confinement ratio and in-pore or at pore-entrance clogging, Formation of Aggregation, Sieving & Arching	[2] [4] [5] [6] [12]

flow due to dominant viscous forces. However, some microflows may be turbulent. So, determining the Reynolds number is essential for microflow analysis. Navier-Stokes Equations (NSE) are widely used in CFD solvers but have limitations for microflows. Continuum assumptions, valid when Knudsen number << 10^{-3}, are challenged due to microflows' small intermolecular distances [9]. In this paper, modelling operates at the boundary of the continuum approach, making it applicable to microflows. NSE assume Newtonian fluid behaviour and constant thermophysical properties, applicable in this isothermal study. Particle-fluid interactions involve various forces, including DLVO forces, gravitational forces, and fluid impact [10].

In membrane flow problems, commercial CFD packages are limited for modeling pore geometry. This study employs a four-way coupling method with CFD and DEM to simulate particle dynamics and interactions within microchannel. Soft-particle models allow deformations and overlapping, suitable for clustering and arching modelling [11]. Surface forces, including drag, are crucial, with the Di Felice Drag Coefficient Method applied. Particle collisions' short time scale is a modelling challenge. STAR-CCM+ employs a spring-damper system for contact forces The Hertz Mindlin model accounts for deformation and friction between colliding spheres [12]. Particle-wall interaction is vital for clogging, simulated using the particle-wall link model, assuming constant high hydrophobicity forces [13]. DEM time step stability is proportional to particle properties [14]. Coupling DEM with CFD is experience-based, often using a ratio of 100 between CFD and DEM time steps [10]. Equation (1) shows the DEM-CFD time step coupling criteria.

$$\Delta t_{CFD} = 100 \Delta t_{DEM} \tag{1}$$

3. Method

A concise overview of the methods used to simulate and investigate microfiltration membrane clogging is provided, including geometry, meshing, simulations settings, and particle injection. The methodology covers solver validation and cake layer thickness approximation. Two stages of numerical modelling are involved: validation and parametric study.

CAD modelling and meshing used Star CCM+, with automated Quad lateral meshing. For 2-D models, 3-D surfaces were split to accommodate 2-D meshing. DEM meshing depended on particle size, following a criterion suggesting the mesh base size should be 3 - 4 times the particle size for stability [10]. The minimum mesh base size was set to 100% of the base mesh size.

Validation emulated an experimental study by [9], involving 5 μm diameter particles injected into a 140 μm wide symmetrical segment of a dead-end filtration device as shown in **Figure 1**. Two injection methods were used: batch and volume flow rate injection. The parametric study focused on cross-flow filtration as shown in **Figure 2** with additional Concentrate region. Volume flow rates were calculated for a dispersion volume fraction of 25%.

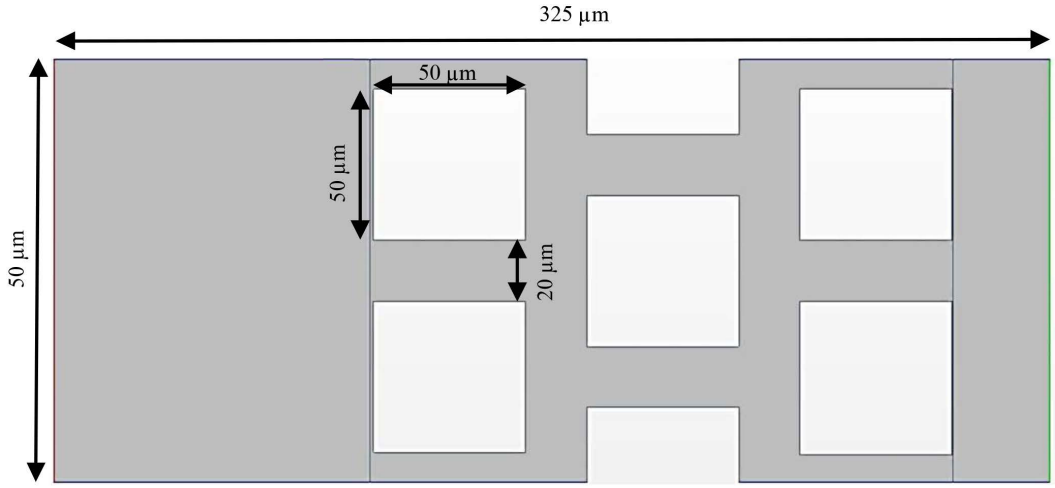

Figure 1. The geometry used for the validation model.

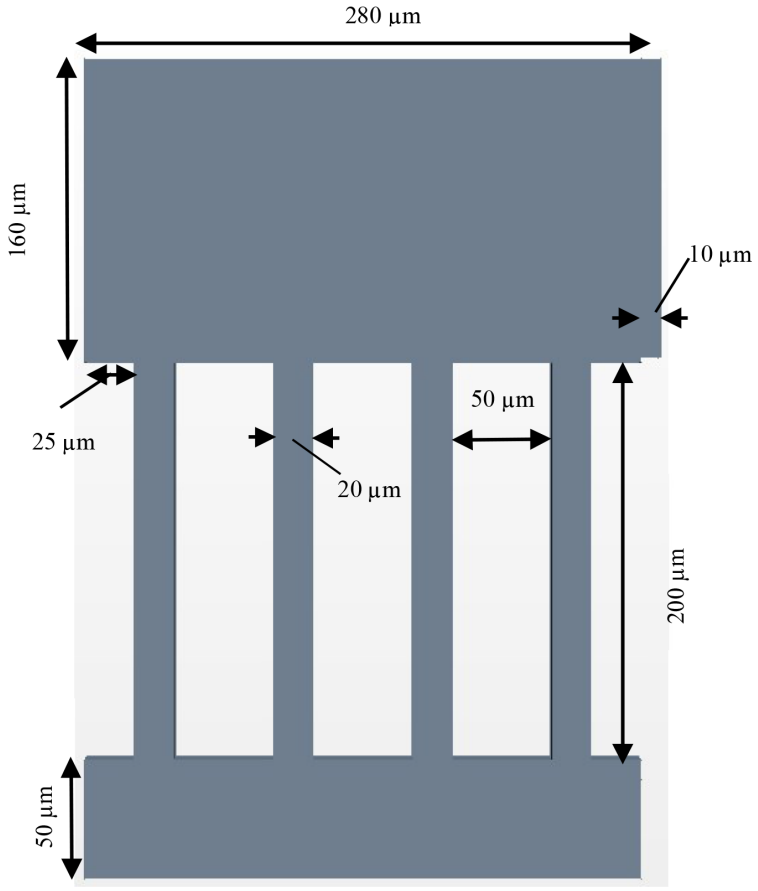

Figure 2. Geometry used for parametric study cases.

For CFD-DEM coupling, Star CCM+ was chosen, optimizing models and settings to align with computational constraints and study objectives. Two-dimensional (2-D) models were utilized due to their efficiency in capturing trends in DEM-CFD simulations [15]. The Lagrange Phase Model facilitated precise control over particle injection.

To balance accuracy and computational cost, the Implicit Unsteady model with sub-stepping was employed, providing a reasonable compromise [16]. The number of sub-stepping was set to its possible lowest value that the solver allows, which is 10 sub-steps per one-time step. Also, the inner loop was set to perform only one iteration. In fact, even with a very low number of sub-steps, the solver showed a good convergence (residuals of order 10^{-3} - 10^{-4}).

As for particle interactions, they were modelled using the Hertz Mindlin model for particle-particle interactions and the Particle-Wall Link model for particle-wall interactions. Coefficients of restitution, friction, and rolling resistances were set, 0.95 and 0.5 for both friction and rolling resistance [10]. For fluid-particle interaction, only the drag model was used. Fluid flow, simulated as water, employed the segregated solver for incompressible conditions, assuming laminar flow due to small Reynolds numbers (0.98 to 13.68). Gravity was included for completeness, with two-way coupling between fluid and particles, allowing mass and momentum exchange. This coupling facilitated the evaluation of body forces such as drag forces.

To validate the solver, two simulation cases were compared to experimental data [8]. A dimensionless comparison was made using filtration time relative to the initial clogging event. The simulation identified this event using field functions that approximate particle packing thickness based on membrane and particle geometry and the averaged particles' position. Precise output capturing from the solver is used to supplement the confirmation of clogging. Also, the average cake layer thickness approximation was derived from the same field function. The comparison between numerical and experimental data shown in **Figure 3** is displaying a strong initial resemblance with a reasonable numerical

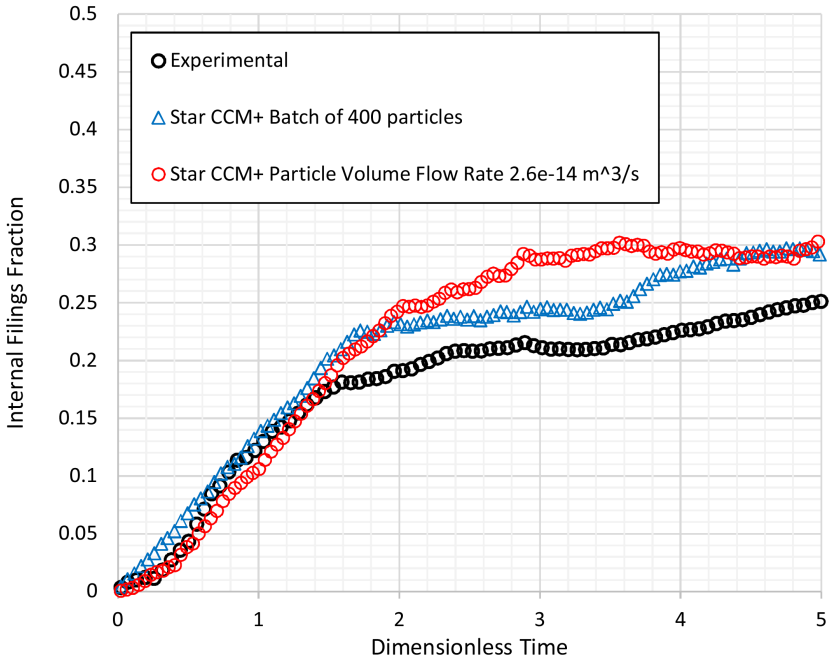

Figure 3. The comparison between numerical and experimental data.

overestimation (around 20% - 30%) of internal fillings beyond 20%. This deviation can be attributed to 2-D model limitations and symmetrical boundary conditions.

Clogging in microfiltration membranes, influenced by time, force, and geometry, was analysed through this parametric study. Investigation was done on membrane geometry, specifically straight pores with varying entrance angles (0˚, 30˚, 45˚, and 60˚), see Figure 4. Hydrodynamic interactions between particles and the continuous phase, driven by fluid momentum, were examined by adjusting mean inlet velocity and trans-membrane flux ratios (75%, 50%, 20%, and 15%). Confinement ratios (4, 3, and 2) were explored by varying particle size (5 μm, 6.66 μm, and 10 μm). 2-D modelling was opted for to reduce computational complexity and offered valuable insights into microfiltration membrane clogging.

4. Results and Discussion

Initially, 18 cases were simulated for 0.025 seconds with 25% particle concentration by volume. Clogging detection in multi-pore microfiltration devices was challenging. Clogging events were visually identified and a clogging index (C_i) introduced. This index categorizes the membrane's clogging status into three categories: No clog, Partial Clog, and Clog, assigning numerical values of 0, 0.5, and 1, respectively. A "Clog" status occurs when at least half of the pores are blocked by persistent clogs, while "Partial Clog" describes clogging in one out of the four pores.

The first parametric test, varying mean inlet velocity, showed partial clogging at higher velocities. An inverse relationship was observed between mean inlet velocity and the cake layer's average thickness as shown in Figure 5. The average thickness of the cake layer for all these cases was fitted in a power function in Figure 6, which was found to provide the best fit across all cases. In high-velocity cases (3 & 7), it is interesting to observe how quickly the cake layer tends to build up, and then almost flattens out. In case 4, there was no particle packing during the simulation explaining its trend.

The second test, investigating trans-membrane flux, revealed a direct proportionality with clogging, but no clear trend in cake layer thickness. This aligned

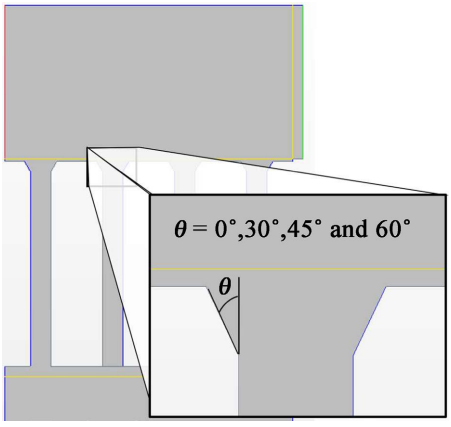

Figure 4. Representation of the entrance angle.

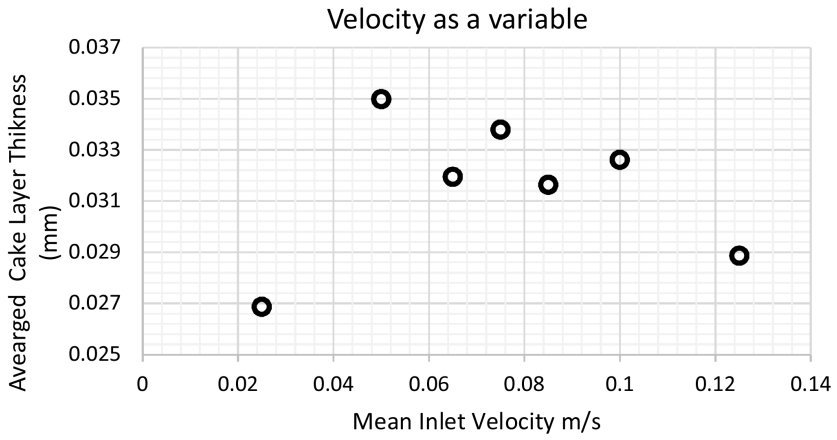

Figure 5. Illustrating the influence of mean inlet velocity on the average thickness of the cake layer.

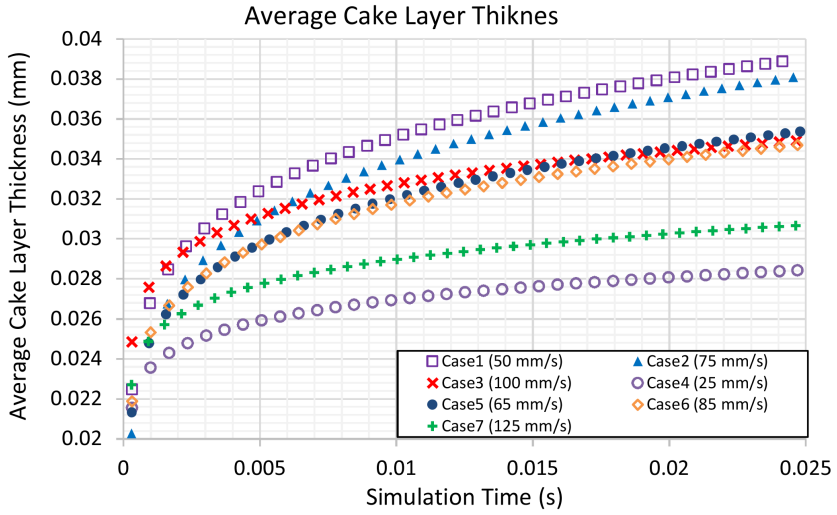

Figure 6. Displaying the averaged thickness of the cake layer growth fitted using a power function.

with the literature. Confinement ratio tests; pore to particle size, done by varying particle size with constant pore size, indicated that a larger confinement ratio reduced clogging likelihood, aligning with previous findings. Higher ratios resulted in in-pore clogging as shown in **Figure 7**, while lower ratios saw entrance clogging as shown in **Figure 8**. The red circles in the figures indicate persistent clog.

Eight cases with four entrance angles were studied. Initially, four cases at a confinement ratio of 3 showed clogging, possibly influenced by this ratio. To mitigate this, a second set of cases with a higher ratio (3 and 12 - 18) was examined. Clear trends weren't apparent at a ratio of 3, possibly due to the lack of a DEM particle restitution coefficient based on impact angle [17]. The influence of the confinement ratio can't be ruled out. However, cases with a ratio of 4 exhibited variability in entrance angles, suggesting an expected upward trend in clogging. Another perspective hints at an inverse relationship with the cosine of the

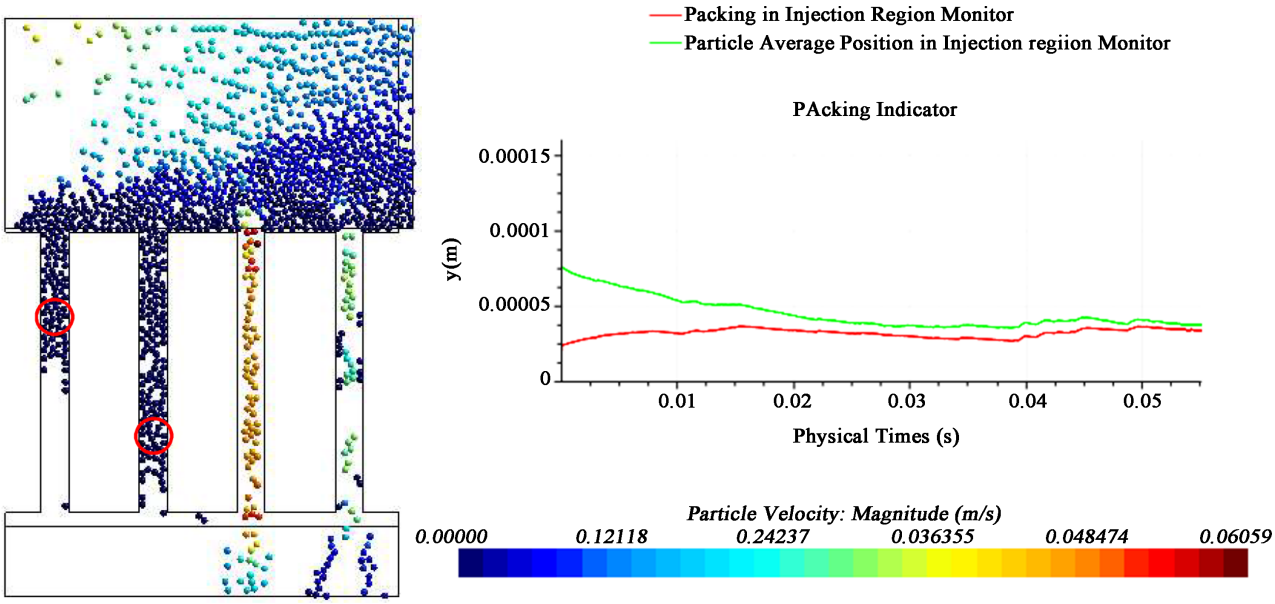

Figure 7. Simulation snapshot showing clogging within pores for a higher confinement ratio case.

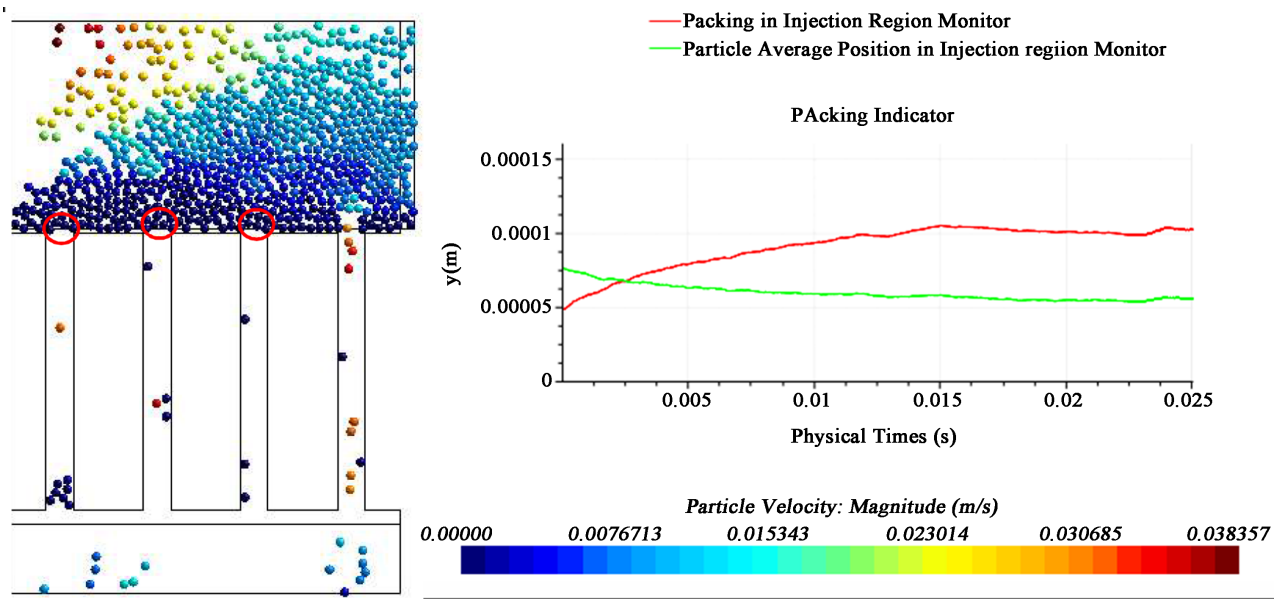

Figure 8. Simulation snapshot displaying clogging at the pore entrance for a lower confinement ratio.

entrance angle, consistent with experimental findings [4].

A parameter based on the presented variables is proposed to quantitatively describe microfiltration membrane clogging. Before exploring this further, Table 2 summarizes observations from the parametric study. Although filtration time hasn't been discussed, it's likely directly related to clogging. Reynolds number (*Re*) was used instead of mean inlet velocity since there is no change in thermophysical properties in all cases, and this approach takes advantage of its dimensionless form. Equation (2) defines a characteristic time for membrane clogging (τ_{clog}). This parameter effectively distinguishes clogging from no clogging, although partial clogging overlaps with both regions. To approximate the

Table 2. Clogging relationship to selected parameters.

Parameter	Clogging
Fluid Reynold Number (*Re*)	Direct
Trans-membrane flux percentage ($\frac{m_{trans}}{m_{Total}} = \beta$)	Direct
Confinement ratio ($W_{pore}/d_{particle} = \gamma$)	Inverse
Cosine of entrance angle ($\cos\theta$)	Inverse
Filtration Time (t_f)	Direct

boundary, the mean average of τ_{clog} from Partial Clog cases is taken and identified as a critical clogging point, which was found to be 0.0589 and was given a symbol ($\tau_{clog\ Criticle}$). Since τ_{clog} is directly proportional to clogging, so its inverse represents the frequency of no clogging events. Therefore, by dividing τ_{clog}^{-1} by ($\tau_{clog\ Criticle}^{-1}$), a description for the relative frequency, *i.e.*, probability of No Clog events can be derived, represented as $P_{No\ Clog}$ and P_{Clog} in Equations (3) and (4).

For $P_{Clog} < 1$, the probability of clogging is impossible, and it is obsolete. Since, P_{Clog} can be a negative value, in such case τ_{clog}. will be below unity for no clog cases, a clogging indicator can be proposed to quantify clogging in easier manners. This indicator is defined as the inverse of the $P_{No\ Clog}$ and it was given the symbol (α) as shown in Equation (5).

$$\tau_{clog} = \frac{Re(\beta)t_f}{\gamma\cos\theta} \tag{2}$$

$$P_{No\ Clog} = \frac{\tau_{clog_{critical}}}{\tau_{clog}} \tag{3}$$

$$P_{Clog} = 1 - \frac{\tau_{clog_{critical}}}{\tau_{clog}} \tag{4}$$

$$\alpha = \frac{\tau_{clog}}{\tau_{clog_{critical}}} = \frac{\tau_{clog}}{0.0589} = 16.98\frac{Re(\beta)t_f}{\gamma\cos\theta} \tag{5}$$

The values of α for all cases, along with parameters listed in Table 2, are presented in Table 3. Notably, in this context, θ represents the entrance angle relative to the vertical axis; otherwise, the equation will yield a negative value. Measuring this angle proves challenging in practice. Additionally, Re is calculated based on the assumed constancy of the inlet mean velocity. This assumption poses a real-world challenge, given that the mean inlet velocity is likely to vary with the growth of the cake layer, significantly impacting the approximation of clogging events. Nonetheless, this model adds value to understanding clogging phenomena. To illustrate this, the clogging indicator (α) was plotted as a function of the clogging index (C_i) in Figure 9 to illustrate its significance in distinguishing clogging events. The same was done for the average cake layer thickness in Figure 10.

Table 3. All parameters for all case and presented.

Case	Cosθ	Re	β	γ	C_i	Clog Statues	Ave Cake Layer (mm)	α
1	1.00	5.47	0.75	4	0.0	No	0.03498	0.44
2	1.00	8.21	0.75	4	0.0	No	0.03380	0.66
3	1.00	10.94	0.75	4	0.5	Partial	0.03260	0.88
4	1.00	2.74	0.75	4	0.0	No	0.02687	0.22
5	1.00	7.11	0.75	4	0.0	No	0.03195	0.57
6	1.00	9.30	0.75	4	0.0	No	0.03164	0.74
7	1.00	13.68	0.75	4	0.5	Partial	0.02887	1.10
8	1.00	10.94	0.50	3	0.5	Partial	0.03153	0.78
9	1.00	10.94	0.20	3	0.0	No	0.03383	0.31
10	1.00	10.94	0.15	3	0.0	No	0.03017	0.23
11	1.00	10.94	0.75	2	1.0	clog	0.06789	1.75
12	1.00	10.94	0.75	3	1.0	clog	0.05933	1.17
13	0.87	10.94	0.75	3	1.0	clog	0.04517	1.35
14	0.71	10.94	0.75	3	1.0	clog	0.04528	1.65
15	0.50	10.94	0.75	3	1.0	clog	0.04636	2.33
16	0.87	10.94	0.75	4	0.5	Partial	0.03459	1.01
17	0.71	10.94	0.75	4	0.5	Partial	0.03702	1.24
18	0.50	10.94	0.75	4	1.0	clog	0.03398	1.75

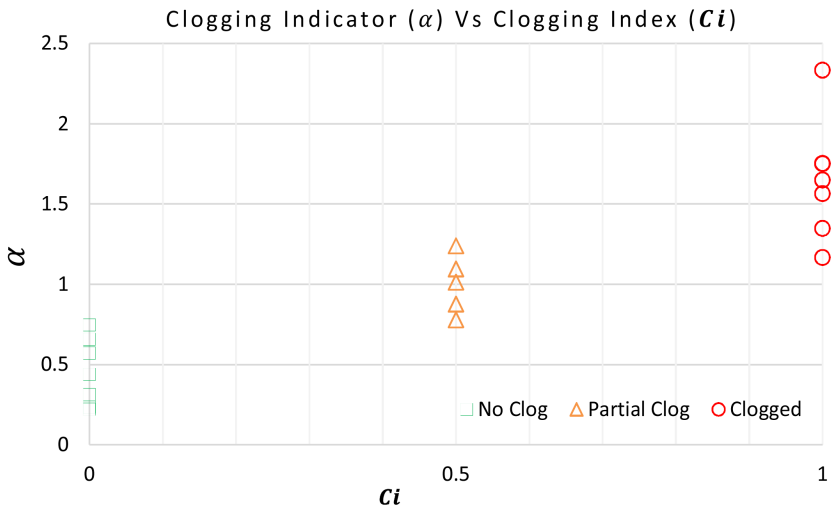

Figure 9. Clogging indicator (α) was plotted as a function of the clogging index C_i.

The main hypothesis of this study is that clogging occurs when $\alpha > 1$, and vice versa. This hypothesis can be extended to include other parameters, such as dispersion volume fraction and temperature, by deriving their dimensionless forms

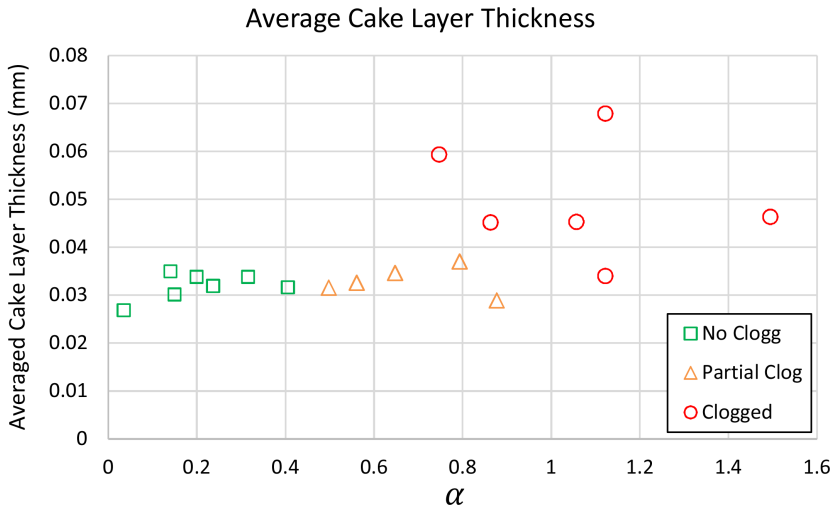

Figure 10. Clogging indicator (a) plotted as a function of the cake layer thickness.

Table 4. Results data for the additional cases.

Case	Cosθ	Re	t_f	β	γ	α	C_i
19	1.00	9.3	0.050	0.75	4	1.5	1
20	1.00	13.68	0.026	0.75	4	1.2	0.5
21	1.00	13.68	0.037	0.75	4	1.7	1

and incorporating them into the calculation of a in Equation (5). While all hypotheses are susceptible to errors, this study acknowledges certain compromises, such as using a 2D modelling approach and the Particle-Wall link model, which affect the level of accuracy achieved. Nevertheless, the analysis provides meaningful results consistent with prior research findings.

To assess the hypothesis, three additional test cases were conducted (Cases 19, 20, and 21) that were initially categorized as "No Clog" but ran until their a values exceeded the critical clogging threshold of unity. Results and data from these cases are presented in **Table 4**. Despite an unexpected outcome of not experiencing a complete clog in Case 20, the hypothesis remains valid, as no clogging occurred with $a < 1$ in any of the cases analysed in this study. **Figure 11** shows a snapshot of case 19 (Re = 9.3, u = 0.085 m/s) at a simulation time of approximately 0.053 seconds. It shows clogging event in the second and last pores from the left-hand side. The time of clogging is approximated to be around 0.05 seconds. **Figure 12** shows a snapshot of case 20 (Re = 13.68, u = 0.125 m/s) at a simulation time of approximately 0.027 seconds. It also shows partial clogging, in which one clogging event took place at the entrance of the last pore to the right. The time of clogging is anticipated to be approximately 0.02625 seconds. Finally, **Figure 13** shows a snap shot of case 21 (Re = 13.68, u = 0.125 m/s) at a simulation time of approximately 0.04125 s. It shows clogging of the membrane by an in-pore clogging in the first pore from the left-hand side and a clogging on the entrance of the last pore to the right. Time of clogging is approximated to be

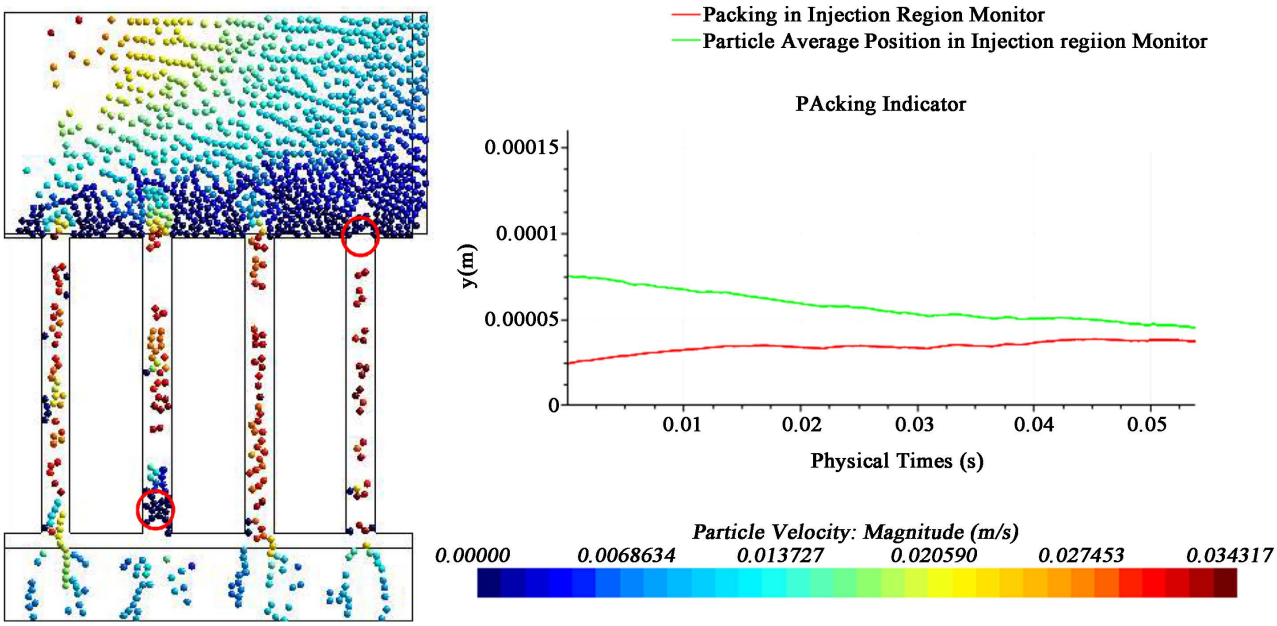

Figure 11. Is a snapshot of case 19 ($Re = 9.3$, $u = 0.085$ m/s).

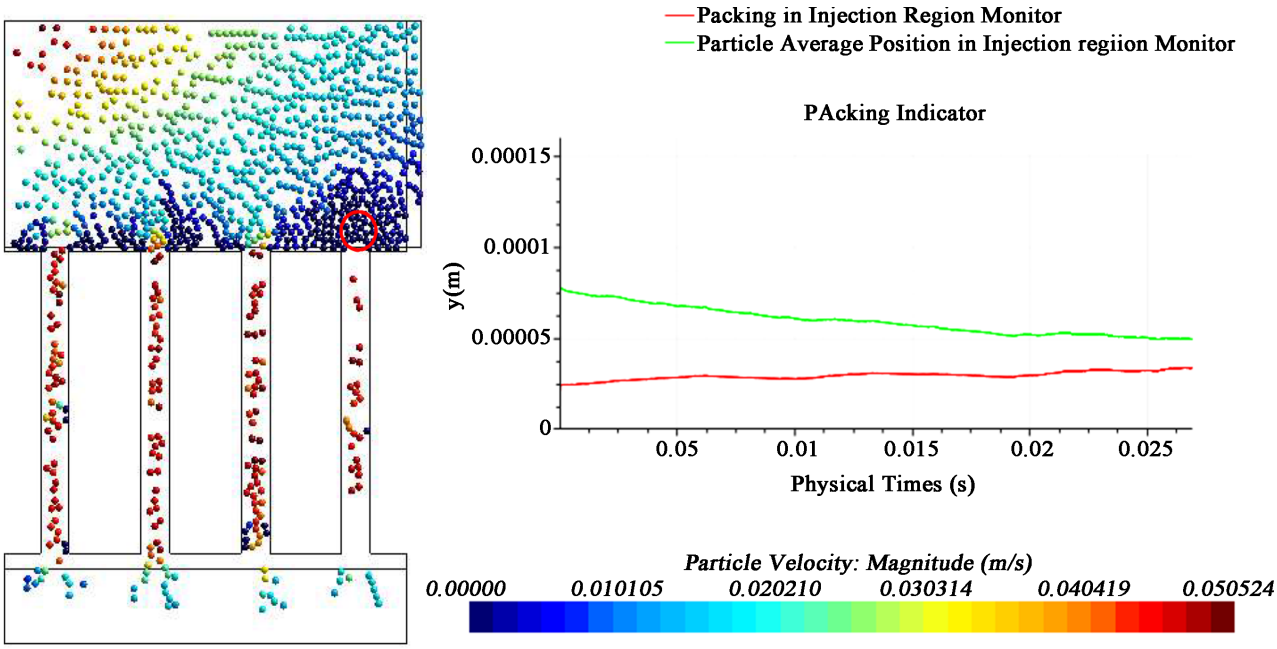

Figure 12. A snapshot of case 20 ($Re = 13.68$, $u = 0.125$ m/s).

around 0.04 s.

5. Conclusion

In this study, the primary goal was to investigate flow-induced clogging factors in microfiltration membranes using computational models. It began by validating the used numerical model against experimental data, achieving approximately 25% consistency with the experimental results. Subsequently, it conducted a comprehensive parametric study using a cross-flow model to explore

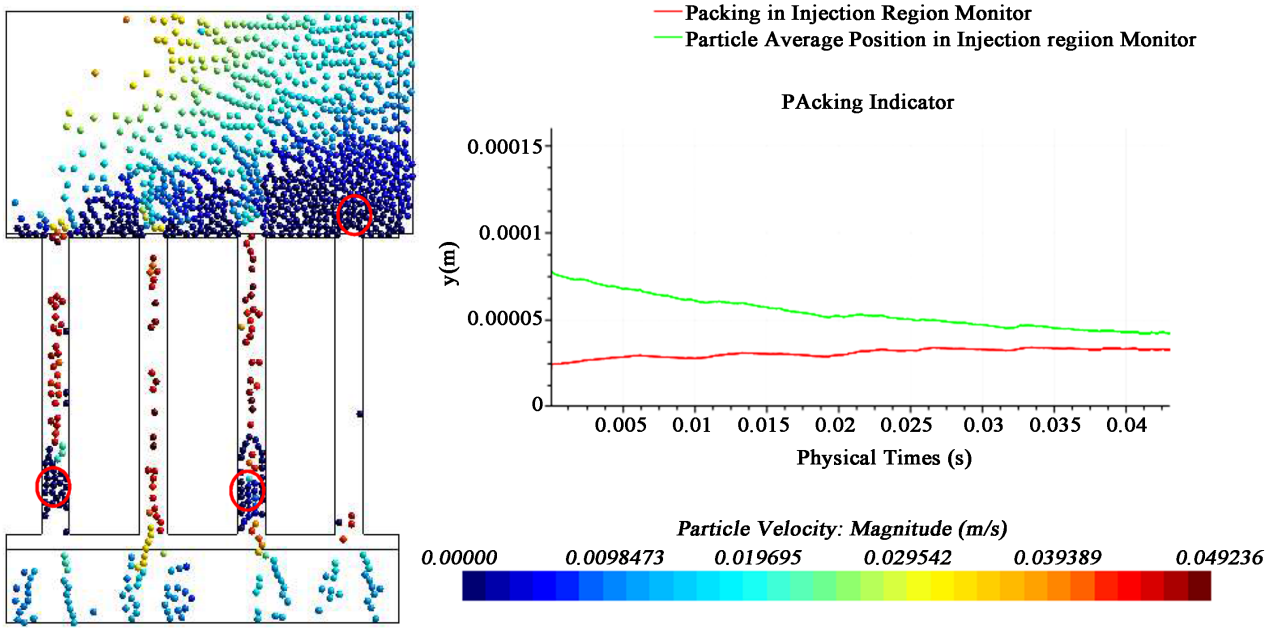

Figure 13. Shows a snap shot of case 21 ($Re = 13.68$, $u = 0.125$ m/s).

selected parameters. Findings revealed several key relationships. Inlet velocity and flux exhibited a direct proportionality with clogging, while the confinement ratio and the cosine of the entrance angle showed an inverse relationship. The growth rate of the cake layer was found to be linked to inlet velocity. Two types of clogging were identified: internal and external, primarily determined by the confinement ratio. To quantify clogging events, a dimensionless clogging indicator (a) was introduced. Looking ahead, future studies should delve into the exploration of various clogging indicators, pore geometry variations, and advanced modelling techniques to enhance accuracy. Calibration of the numerical filtration time and the consideration of particle volume fraction are pivotal for more precise results. Additionally, the adoption of 3D models is recommended to improve overall accuracy.

Acknowledgements

This research paper builds upon the master's dissertation submitted to the University of Manchester, as part of the requirements for the Master of Science in Thermal Power and Fluid Engineering degree. The original work serves as the basis for the insights presented in this paper, with recognition given to the University of Manchester for providing an environment conducive to academic inquiry.

Conflicts of Interest

The author declares no conflicts of interest regarding the publication of this paper.

References

[1] Li, N.N., Fane, A.G., Winston Ho, W.S. and Matsuura, T. (2008) Advanced Membrane Technology and Applications. John Wiley & Sons, Inc., Hoboken, NJ.

[2] van Zwieten, R., van de Laar, T., Sprakel, J. and Schroën, K. (2018) From Cooperative to Uncorrelated Clogging in Cross-Flow Microfluidic Membranes. *Scientific Reports,* **8**, Article No. 5687. https://doi.org/10.1038/s41598-018-24088-6

[3] Rahimia, M., Madaenia, S.S., Abolhasania, M. and Alsairafib, A.A. (2009) CFD and Experimental Studies of Fouling of a Microfiltration Membrane. *Chemical Engineering and Processing,* **48**, 1405-1413. https://doi.org/10.1016/j.cep.2009.07.008

[4] van de Laar, T., Ten Klooster, S., Schroën, K. and Sprakel1, J. (2016) Transition-State Theory Predicts Clgging at the Microscal. *Scientific Reports,* **6**, Article No. 28450. https://doi.org/10.1038/srep28450

[5] Dressaire, E. and Sauret, A. (2017) Clogging of Microfluidic Systems. *Soft Matter,* **13**, 37-48. https://doi.org/10.1039/C6SM01879C

[6] Andoa, T., Akamatsub, K., Nakao, S.-I. and Fujitac, M. (2012) Simulation of Fouling and Backwash Dynamics in Dead-End Microfiltration. *Journal of Membrane Science,* **392-393**, 48-57. https://doi.org/10.1016/j.memsci.2011.11.051

[7] Smuts, E.M., Deglon, D.A. and Meyer, C.J. (2012) Methodology for CFD-DEM Modelling of Particulate Suspension Rheology. In *Proceedings of the Ninth International Conference on CFD in the Minerals and Process Industries*, Melbourne, 10-12 December 2012. https://www.cfd.com.au/cfd_conf12/index.html

[8] Bacchin, P., Derekx, Q., Veyret, D., Glucina, K. and Moulin, P. (2014) Clogging of Microporous Channels Networks: Role of Connectivity and Tortuosity. *Microfluidics and Nanofluidics,* **17**, 85-96. https://doi.org/10.1007/s10404-013-1288-4

[9] Addae-Mensah, K.A., Wang, Z.K., Parsa, H., Chin, S.Y., Laksanasopin, T. and Sia, S.K. (2010) Fundamentals of Microfluidics Devices. In: Kumar, C.S., Ed., *Microfluidic Devices in Nanotechnology*: *Fundamental Concepts*, John Wiley & Sons, Inc., 1-38. https://doi.org/10.1002/9780470622636.ch1

[10] Lohausa, J., Pereza, Y.M. and Wesslinga, M. (2018) What Are the Microscopic Events of Colloidal Membrane Fouling? *Journal of Membrane Science,* **553**, 90-98. https://doi.org/10.1016/j.memsci.2018.02.023

[11] Norouzi, H.R., Reza, Z., Sotudeh-Gharebagh, R. and Mostoufi, N. (2016) DEM Formulation. In: *Coupled CFD-DEM Modeling*: *Formulation, Implementation and Application to Multiphase Flows*, John Wiley & Sons, Ltd., Chichester, 15-67. https://doi.org/10.1002/9781119005315.ch2

[12] Saxena, V., Krief, M. and Adam, L. (2018) Handbook of Borehole Acoustics and Rock Physics for Reservoir Characterization. Elsevier.

[13] Siemens PLM Software (2023) StarCCM+ User Guide: Particle-Wall Link Model Reference (Version 14.06). Siemens PLM Software

[14] Gu, Y., Ozel, A. and Sundaresan, S. (2016) A Modified Cohesion Model for CFD-DEM Simulations of Fluidization. *Powder Technology,* **296**, 17-28. https://doi.org/10.1016/j.powtec.2015.09.037

[15] Shahzad, K., D'Avino, G., Greco, F., Guido, S. and Maffettone, P.L. (2016) Numerical Investigation of Hard-Gel Microparticle Suspension Dynamics in Microfluidic Channels: Aggregation/Fragmentation Phenomena, and Incipient Clogging. *Chemical Engineering Journal,* **303**, 202-216. https://doi.org/10.1016/j.cej.2016.05.134

[16] Versteeg, H.K. and Malalasekera, W. (2007) An Introduction to Computational Fluid Dynamics. 2nd Edtiton, Pearson Education, London.

[17] Lindberg, S. (2015) Numerical Simulation of Particle Soiling in the Engine Compartment of a Bus. Master's Thesis, Chalmers University of Technology, Göteborg. https://publications.lib.chalmers.se/records/fulltext/219482/219482.pdf